Journal of Computational Physics **181,** 45–67 (2002)
doi:10.1006/jcph.2002.7128

Modeling and Computation of Random Thermal Fluctuations and Material Defects in the Ginzburg–Landau Model for Superconductivity

Jennifer Deang,*[,1] Qiang Du,† and Max D. Gunzburger‡

*Department of Mathematics, Virginia Polytechnic Institute and State University, Blacksburg, Virginia 24060-0123; †Department of Mathematics, Pennsylvania State University, University Park, Pennsylvania 16802; and ‡Department of Mathematics, Iowa State University, Ames, Iowa 50011-2064

Received June 4, 2001; revised May 31, 2002

It is well known that thermal fluctuations and material impurities affect the motion of vortices in superconductors. These effects are modeled by variants of a time-dependent Ginzburg–Landau model containing either additive or multiplicative noise. Numerical computations are presented that illustrate the effects that noise has on the dynamics of vortex nucleation and vortex motion. For an additive noise model with relatively low variances, it is found that the vortices form a quasi-steady-state lattice in which the vortex core sizes remain roughly fixed but their positions vibrate. Two multiplicative noise models are considered. For one model having relatively long-range order, the sizes of the vortex cores vary in time and from one vortex to another. Finally, for the additive noise case, we show that as the variance of the noise tends to zero, solutions of the stochastic time-dependent Ginzburg–Landau equations converge to solutions of the corresponding equations with no noise.

Key Words: noise; superconductivity; finite element methods; fluctuations.

1. INTRODUCTION

The mathematical and computational study of phenomenological Ginzburg–Landau models for low-temperature superconductivity has received much attention in recent years. The partial differential equations which define the models involve the complex-valued order parameter ψ, the vector-valued magnetic potential $\mathbf{A}$, and the scalar-valued electric potential Φ. Recent studies have provided rigorous justifications concerning the vortex

[1] Current address: Lockheed Martin Mission Systems, 700 North Frederick Avenue, Gaithersburg, MD 20879.

0021-9991/02 $35.00

state in type-II superconductors which were previously understood only based on physical heuristics and observations. However, the mathematical formulations of the conventional Ginzburg–Landau theory are applicable only to highly idealized physical contexts that do not take into account factors such as inhomogeneities, thermal fluctuations, and random applied fields. For example, it is well known that thermal fluctuations and material defects play a central role in the pinning of vortices in type-II superconductors [16, 21]. It is also well known that as the temperature approaches the transition temperature and the effect of thermal fluctuations increases, the vortex lattice melts and there is a transition to a vortex-liquid state; see [17] for recent convincing experimental evidence. Thus, studies of the stability, dynamics, interactions, and other properties of the vortex state based on deterministic Ginzburg–Landau models do not necessarily carry over to situations for which the above factors cannot be ignored.

In this paper, we develop and apply computational methods that can be used to determine the effects of random thermal fluctuations and material defects on the vortex dynamics in type-II superconductors. The algorithms are based on stochastic versions of the Ginzburg–Landau model. For simplicity, we assume that the underlying material sample possesses a large value for the Ginzburg–Landau parameter κ so that a reduction of the Ginzburg–Landau equations to their high-κ limit can be employed [2, 8]. This implies that the given applied field penetrates the sample completely, i.e., the induced field is equal to the applied field and is independent of the sample properties. We will consider different forms for the noise in the high-κ limit model. We will then develop algorithms for discretizing the noise and illustrate, through numerical experiments, their effect on the dynamics of the nucleation of vortices.

The paper is organized as follows. In the remainder of this section, we discuss some notions about random fields and stochastic processes. In Section 2, we introduce stochastic variants of the high-κ Ginzburg–Landau model which involve either additive or multiplicative noise. In Section 3, we discuss the discretization of noise. Then, in Section 4, we present the results of some numerical experiments with additive noise models and, in Section 5, we do likewise for multiplicative noise models. In Section 6, we examine the large time behavior of the vortex motion and, in Section 7, we look at theoretical issues related to the large time behavior and the small variance limit of such motions. Finally, in Section 8, we give a summary of our findings and some concluding remarks.

1.1. Random Fields and Stochastic Processes

In n-dimensional space, locations are denoted by a vector $\mathbf{v} = (v_1, \ldots, v_n)$ whose elements are coordinates or parameters. A random field can be viewed as an indexed family of random variables. The value of a random field at the location $\mathbf{v}$ in parameter space is a random variable. The collective outcome of all experiments comprising the random field is the *realization of the random field*, and its value is the observed outcome at the point $\mathbf{v}$ where the random field is realized. The outcome of the random variable associated with any location $\mathbf{v}$ is also referred to as the *state* of the random field at that location.

We use two types of realizations for random fields.

1. *Continuous random functions*: if observations are made at all points along one or more spatial coordinate axes $(x_1, x_2, \ldots, x_d)$ and/or the time axis t.

2. *Lattice processes*: if observations are made at the nodes or sites of a discrete lattice in space/time.

We take n-dimensional space to be $\mathbb{R}^{d+1}$ to analyze the time-dependent Ginzburg–Landau equations, with d denoting the space dimension ($d = 2, 3$). A continuous random process is used in the strong and weak forms of the Ginzburg–Landau equations with noise that accounts for thermal fluctuations and random material effects, while the lattice process is used in the discretized weak form of the Ginzburg–Landau equations.

2. HIGH κ GINZBURG–LANDAU MODELS WITH NOISE

In the time-dependent *high-κ model* [8], the resulting simplified leading-order system is a nonlinear, complex-valued equation for the leading-order (in terms of $1/\kappa^2$) order parameter ψ_0, where κ denotes the Ginzburg–Landau parameter which is a material property. Most superconductors of practical use have "high" values for κ. The time-independent magnetic potential $\mathbf{A}_0$ is solved for separately from the given applied field $\mathbf{H}_0$ using Maxwell's equations. Thus, throughout, we can assume that $\mathbf{A}_0$ is a given, deterministic vector field.

The derivation of the high-κ model in the deterministic setting starts with the well-known time-dependent Ginzburg–Landau equations [22]. Then, the limit as the Ginzburg–Landau parameter κ goes to infinity is considered, with the applied field assumed to be of order κ. A gauge choice of the type $\Phi = 0$ (where Φ denotes the electric potential) in the sample and $\mathbf{A} \cdot \mathbf{n} = 0$ on the boundary of the sample is invoked. The applied current is assumed to be small so that it has no effect on the leading-order behavior of the order parameter. The resulting high-κ model (see [2, 8] for details) is then given by

$$\frac{\partial \psi_0}{\partial t} + (i\nabla + \mathbf{A}_0)^2 \psi_0 - \psi_0 + |\psi_0|^2 \psi_0 = 0 \qquad \text{in } \Omega \tag{1}$$

$$(i\nabla + \mathbf{A}_0)\psi_0 \cdot \mathbf{n} = 0 \qquad \text{on } \Gamma \tag{2}$$

$$\psi_0(\mathbf{x}, 0) = \varphi(\mathbf{x}) \quad \text{in } \Omega, \tag{3}$$

where $\Omega \in \mathbb{R}^d$ denotes the superconducting sample and Γ its boundary. Later, we will drop the subscript 0 that denotes the leading-order variables.

Although at each point in the material and at each instant in time thermal fluctuations or material defects may have a negligible effect, the superposition of many interactions can produce observable effects. The movement of a particular vortex cannot be found exactly; thus, the motion is described statistically. Fluctuations and defects, being random in nature, produce instantaneous changes in the movement of the vortex. In [21], it is argued that these thermodynamic fluctuations are generally quite small which correspond to a small value for the variance. The same could be argued in the case of random material defects.

Noise may be added to the high-κ model in different ways. Here, we consider two approaches: the cases of additive and multiplicative noise. The comparison of these two types of noise models in other physically meaningful systems has received much attention; see, e.g., [15].

2.1. Additive Noise High-κ Model

The additive noise high-κ Ginzburg–Landau model that we use is a simple modification of the deterministic high-κ Ginzburg–Landau model (1)–(3). Following [14], we introduce into the right-hand side of (1) a random, continuous, complex-valued field in time and space. In this way, thermal fluctuations are modeled by Langevin-type dynamics. More detailed

physical interpretations of additive noise random fields can be found in [14, 20]. Thus, the additive noise high-κ Ginzburg–Landau model is given by

$$\frac{\partial \psi}{\partial t} + (i\nabla + \mathbf{A})^2\psi - \psi + |\psi|^2\psi = \eta \qquad \text{in } \Omega \tag{4}$$

$$(i\nabla + \mathbf{A})\psi \cdot \mathbf{n} = 0 \qquad \text{on } \Gamma \tag{5}$$

$$\psi(\mathbf{x}, 0) = \varphi(\mathbf{x}) \quad \text{in } \Omega, \tag{6}$$

where η is a random, continuous, complex-valued field in time and space. In the context of Ginzburg–Landau models, the additive noise-induced Langevin dynamics have been studied in [6, 13, 23, 24] in which analytical methods are used to study the transition between the disordered vortex-lattice and normal states; these papers do not specifically monitor the vortex-liquid state which is intermediate between the vortex-glass and normal states. In this paper, we use computational techniques to study the details of the full transition through the vortex-glass, vortex-liquid, and normal states as the temperature is increased.

The random source term η is assumed to be noise generated by an infinite-dimensional Brownian motion; see [4] for a more precise definition. If this stochastic term is meant to model the effects of thermal fluctuations, then its variance σ is, of course, temperature dependent. In fact, we have that $\sigma = K(T/T_c)(1 - T/T_c)^{-2}$, where T and T_c denote the temperature and the critical transition temperature, respectively, and K is a temperature-independent constant. (Using the experimental results of [17], one can glean that, very roughly, $K \approx 1/80$.) Note that the variance tends to infinity as $T \to T_c$, which is to be expected; i.e., when the temperature is very close to the transition temperature, the effects of thermal fluctuations should be large.

We note that in the system (4)–(6), the space variables have been nondimensionalized with respect to the temperature-dependent coherence length, i.e., with respect to $\xi(T) = \xi(0)(1 - T/T_c)^{-1/2}$. In our computational simulations, we will vary the variance of the noise or, equivalently, we will vary the temperature. As a result, because of our nondimensionalization scale, changing the variance implies that we are also changing ξ. This means that as we change the value of variance, the spatial scale used for nondimensionalization changes. The relation between ξ and σ is easily found to be $(\xi(T)/\xi(0))^2 = (1 + \sqrt{1 + 4\sigma/K})/2$ so that for large values of σ we have that $\xi(T) \propto \sigma^{1/4}$. Thus, for example, doubling the variance in our computational simulations means that, for large variances, we are enlarging the linear dimension of the material sample by a factor of 1.19. It should be noted that the scale used for nondimensionalizing the time is also temperature dependent.

The set of time-dependent equations (4)–(6) for ψ is now nondeterministic in nature. The resulting equation for ψ with additive noise can also be given in the abstract form

$$du(t) = \hat{A}(u(t))\,dt + \sigma\,dW(t) \tag{7}$$

along with the initial condition

$$u(0) = \varphi, \tag{8}$$

where $u(t) = \psi(t)$; $\hat{A}$ is the operator $\hat{A} = \hat{A}_0 + F$, where

$$F(u) = u - |u|^2 u \tag{9}$$

is a monotone nonlinear operator and $\hat{A}_0$ is a linear differential operator defined by

$$\hat{A}_0 u = (\nabla - i\mathbf{A})^2 u \tag{10}$$

for u satisfying

$$(\nabla - i\mathbf{A})u \cdot \mathbf{n} = 0 \quad \text{on } \Gamma. \tag{11}$$

In (7), σ is a positive parameter and $W(t)$ denotes a *Hilbert space-valued* Wiener process. This abstract form of the time-dependent Ginzburg–Landau equations with thermal fluctuations will be studied in Section 7.

2.2. Multiplicative Noise High-κ Model

The multiplicative noise model we study corresponds to the following abstract form:

$$du(t) = \hat{A}(u(t))\,dt + \sigma u(t)\,dW(t). \tag{12}$$

Physically, multiplicative noise has been used to model the effects of the inhomogeneity of the effective interactions between electrons; for details, see, e.g., [16]. In the high-κ Ginzburg–Landau setting, the corresponding stochastic model is given by

$$\frac{\partial \psi}{\partial t} + (i\nabla + \mathbf{A})^2\psi - \psi + |\psi|^2\psi = \eta\psi \qquad \text{in } \Omega \tag{13}$$

$$(i\nabla + \mathbf{A})\psi \cdot \mathbf{n} = 0 \qquad \text{on } \Gamma \tag{14}$$

$$\psi(\mathbf{x}, 0) = \varphi(\mathbf{x}) \quad \text{in } \Omega, \tag{15}$$

Again, the variance of the noise coefficient η is inversely related to the difference between the temperature and the critical temperature of transition between the superconducting and normal states.

If the noise coefficient η models defects in the material sample, then the nature of the noise depends on the scale of the inhomogeneities. If these are smaller than a Ginzburg–Landau coherence length ξ, one may assume that η is independent in space and time. On the other hand, if the inhomogeneities are correlated over distances comparable to a coherence length, then the coefficient η should have a similar correlation length scale.

If the noise coefficient η models the effects of thermal fluctuations, then it is not clear what the nature of the noise should be. Furthermore, it is not clear if multiplicative noise models satisfy the fluctuation–dissipation theorem; see [14]. Indeed, one of the goals of this paper is to develop computational algorithms that can be used to examine the effects of different noise models on the dynamics of vortices. Hopefully, by examining those dynamics one can gain some insight into which noise models are likely to be correct.

3. DISCRETIZED NOISE MODELS

The noise models we have introduced involve continuous random functions in space and time. To carry out some computational simulations, we must discretize these random

functions. Relevant to the following discussion is the observation that the high-κ Ginzburg–Landau model we are using has been nondimensionalized with respect to the Ginzburg–Landau coherence length ξ so that unit distances in that model correspond to a coherence length scale.

For the additive noise model we have assumed that η is independent in space and time. As a result, for that model we approximate η by a grid function whose nodal values at all grid points and time steps are sampled as independent random variables with a Gaussian distribution of zero mean and variance σ. Consequently, if one refines the grid used for the solution of (4)–(6) one also refines the sampling points for the approximation of η.

For the numerical approximation of the multiplicative noise model, we will use two types of discretized noise. First, we will use a discretized noise similar to that used in the additive noise case. This models noise that is correlated over length scales smaller than the coherence lenght. We will also use discretized noise that is sampled on a lattice that is fixed with respect to the grid used to discretize (13)–(15). This models noise that is correlated over length scales comparable to the coherence length.

We now give some additional details concerning the discretization of noise in the context of finite element methods.

3.1. Discretization of Space–Time-Independent Additive Noise

We discuss the discretization of space–time-independent noise in the additive noise case. For a thorough discussion of finite element discretizations of deterministic Ginzburg–Landau models, see [7, 9, 10]. Here we will only discuss issues directly relevant to the introduction of noise into Ginzburg–Landau models.

To effect a finite element discretization of (4)–(6), we choose a finite element space V^h with basis $\{\phi_j^h(\mathbf{x})\}_{j=1}^J$, e.g., continuous piecewise quadratic polynomials with respect to a triangulation of Ω. At each time step $n = 0, 1, 2, \ldots$, we seek an approximate solution of the form

$$\psi_h^{(n)}(\mathbf{x}) = \sum_{j=1}^{J} c_j^{(n)} \phi_j^h(\mathbf{x}),$$

where, for each n, $\{c_j^{(n)}\}_{j=1}^J$ is the set of complex-valued coefficients to be determined. Thus, we have that

$$\psi_h^{(n)}(\mathbf{x}) \approx \psi(\mathbf{x}, n\Delta t) \quad \text{for } \mathbf{x} \in \Omega.$$

For $n = 0$, we determine $\{c_j^{(0)}\}_{j=1}^J$ from the initial condition $\psi(\mathbf{x}, 0) = \varphi(\mathbf{x})$.

For $n = 1, 2, \ldots$, we determine $\{c_j^{(n)}\}_{j=1}^J$ from the discretized weak form of (4)–(6), i.e., from

$$\begin{aligned}
&\int_\Omega \left(\frac{\psi_h^{(n)} - \psi_h^{(n-1)}}{\Delta t}, \tilde{\psi}_h^* \right) d\Omega + \int_\Omega \left(i\nabla\psi_h^{(n)} + \mathbf{A}\psi_h^{(n)} \right) \cdot \left(-i\nabla\tilde{\psi}_h^* + \mathbf{A}\tilde{\psi}_h^* \right) d\Omega \\
&\quad - \int_\Omega \left(\psi_h^{(n)} + \left|\psi_h^{(n)}\right|^2 \psi_h^{(n)} \right) \tilde{\psi}_h^* \, d\Omega \\
&\quad = \int_\Omega \eta_h^{(n)} \tilde{\psi}_h^* \, d\Omega \quad \forall \tilde{\psi}_h \in V^h,
\end{aligned} \tag{16}$$

where we have used a backward Euler discretization in time. Actually, the integrals in (16) are not evaluated exactly, but instead, quadrature rules are used; for example, we would use the approximation

$$\int_\Omega \eta_h^{(n)} \tilde{\psi}_h^* \, d\Omega \approx \sum_{e=1}^{E} \sum_{q=1}^{Q} w_{e,q} \eta_h^{(n)}(\mathbf{x}_{e,q}) \tilde{\psi}_h^*(\mathbf{x}_{e,q}),$$

where E is the number of triangles, $e = 1, \ldots, E$ is an indexing of the triangles, Q is the number of quadrature points in each triangle, $w_{e,q}$ for $q = 1, \ldots Q$ are the quadrature weights in triangle e, and $\mathbf{x}_{e,q}$ for $q = 1, \ldots Q$ are the quadrature points in triangle e.

One way to discretize the noise is given by

$$\eta_h^{(n)}(\mathbf{x}) = \sum_{j=1}^{J} \nu_j^{(n)} \phi_j^h(\mathbf{x}), \tag{17}$$

where, for each j and each n, $\nu_j^{(n)}$ is chosen randomly from a Gaussian distribution with mean zero and variance σ. Essentially, at each time step n, a new set of nodal values $\{\nu_j^{(n)}\}_{j=1}^J$ is chosen randomly from the Gaussian distribution; the values of the noise at other points in Ω are then determined by interpolation through (17). As a result, the noise term in the discrete equation (16) is approximated by

$$\int_\Omega \eta_h^{(n)} \tilde{\psi}_h^* \, d\Omega \approx \sum_{e=1}^{E} \sum_{q=1}^{Q} \sum_{j=1}^{J} w_{e,q} \nu_j^{(n)} \phi_j^h(\mathbf{x}_{e,q}) \tilde{\psi}_h^*(\mathbf{x}_{e,q}).$$

Note that when one refines the temporal and/or spatial grid one also refines the sampling points for $\nu_j^{(n)}$.

An alternate way to discretize the noise is given by

$$\eta_h^{(n)}(\mathbf{x}_{e,q}) = \mu_{e,q}^{(n)}, \tag{18}$$

where for each time step n, each triangle e, and each quadrature point q, $\mu_{e,q}^{(n)}$ is chosen randomly from a Gaussian distribution with mean zero and variance σ. Now, at each time step n, we are choosing the noise randomly from the Gaussian distribution at each quadrature point in each triangle. Thus, the noise term in the discrete equations is now approximated by

$$\int_\Omega \eta_h^{(n)} \tilde{\psi}_h^* \, d\Omega \approx \sum_{e=1}^{E} \sum_{q=1}^{Q} w_{e,q} \mu_{e,q}^{(n)} \tilde{\psi}_h^*(\mathbf{x}_{e,q}).$$

Again, when one refines the temporal and/or spatial grids one also refines the sampling points for $\mu_{e,q}^{(n)}$. In fact, the two ways (17) and (18) of discretizing noise discussed so far are basically equivalent; i.e., in both cases, the distribution is sampled at points and times whose spacing is determined by the grids used in the discretization of the partial differential equations. Thus, as the spacial and temporal grids are refined, the distribution is sampled on commensurately finer scales. Furthermore, the two methods yield very similar numerical results.

3.2. Discretization of Space–Time-Independent and Correlated Multiplicative Noise Models

If the multiplicative noise coefficient η is assumed to be independent in space and time, it can be discretized in the same ways as those used for additive noise in Section 3.1. In this case, we have that the finite element approximation of (13)–(15) is determined from

$$\begin{aligned}
&\int_\Omega \left(\frac{\psi_h^{(n)} - \psi_h^{(n-1)}}{\Delta t}, \tilde{\psi}_h^* \right) d\Omega + \int_\Omega \left(i\nabla\psi_h^{(n)} + \mathbf{A}\psi_h^{(n)} \right) \cdot \left(-i\nabla\tilde{\psi}_h^* + \mathbf{A}\tilde{\psi}_h^* \right) d\Omega \\
&\quad - \int_\Omega \left(\psi_h^{(n)} + \left|\psi_h^{(n)}\right|^2 \psi_h^{(n)} \right) \tilde{\psi}_h^* \, d\Omega \\
&\quad = \int_\Omega \eta_h^{(n)} \psi_h^{(n)} \tilde{\psi}_h^* \, d\Omega \quad \forall \tilde{\psi}_h \in V^h,
\end{aligned} \tag{19}$$

where the discretized noise coefficient $\eta_h^{(n)}$ is given by either (17) or (18). Thus, when a quadrature rule is used to approximate the integrals in (19), the right-hand side is respectively approximated by

$$\int_\Omega \eta_h^{(n)} \psi_h^{(n)} \tilde{\psi}_h^* \, d\Omega \approx \sum_{e=1}^{E} \sum_{q=1}^{Q} \sum_{j=1}^{J} w_{e,q} \nu_j^{(n)} \phi_j^h(\mathbf{x}_{e,q}) \psi_h^{(n)}(\mathbf{x}_{e,q}) \tilde{\psi}_h^*(\mathbf{x}_{e,q}),$$

where, for each time step n and for each node j, $\nu_j^{(n)}$ is chosen randomly from the Gaussian distribution, or

$$\int_\Omega \eta_h^{(n)} \psi_h^{(n)} \tilde{\psi}_h^* \, d\Omega \approx \sum_{e=1}^{E} \sum_{q=1}^{Q} w_{e,q} \mu_{e,q}^{(n)} \psi_h^{(n)}(\mathbf{x}_{e,q}) \tilde{\psi}_h^*(\mathbf{x}_{e,q}),$$

where, for each time step n and for each quadrature point $\mathbf{x}_{e,q}$, $\mu_{e,q}^{(n)}$ is chosen randomly from a Gaussian distribution.

If the multiplicative noise coefficient η is assumed to be correlated over scales commensurate with the coherence length, then the space–time grid used to discretize the noise is chosen to be fixed with respect the space–time grid used to discretize the partial differential equation. Then, (19) is replaced by

$$\begin{aligned}
&\int_\Omega \left(\frac{\psi_h^{(n)} - \psi_h^{(n-1)}}{\Delta t}, \tilde{\psi}_h^* \right) d\Omega + \int_\Omega \left(i\nabla\psi_h^{(n)} + \mathbf{A}\psi_h^{(n)} \right) \cdot \left(-i\nabla\tilde{\psi}_h^* + \mathbf{A}\tilde{\psi}_h^* \right) d\Omega \\
&\quad - \int_\Omega \left(\psi_h^{(n)} + |\psi_h^{(n)}|^2 \psi_h^{(n)} \right) \tilde{\psi}_h^* \, d\Omega \\
&\quad = \int_\Omega \eta_{\hat{h},\hat{\Delta}t} \psi_h^{(n)} \tilde{\psi}_h^* \, d\Omega \quad \forall \tilde{\psi}_h \in V^h.
\end{aligned} \tag{20}$$

In (20), $\hat{h}$ and $\hat{\Delta}t$ denote the space–time grid used to discretize the noise coefficient η; they are chosen on a scale comparable to the coherence length. If h and Δt are the spatial and temporal grid sizes used to discretize (13)–(15), then these are small compared with the coherence length; i.e., $h \ll \hat{h}$ and $\Delta t \ll \hat{\Delta}t$.

In (20), the discrete noise $\eta_{\hat{h},\hat{\Delta}t}(\mathbf{x}, t)$ could be defined by sampling a Gaussian distribution at times $\hat{n}\hat{\Delta}t$, $\hat{n} = 0, 1, 2, \ldots$, and at the nodes of a finite element grid having grid size $\hat{h}$;

at other times and at other spatial points, the noise is then determined by interpolation. For example, let $\mu_{\hat{\jmath},\hat{n}}$ be the value of the noise sampled at the time $\hat{n}\hat{\Delta}t$ and at the $\hat{\jmath}$th node of the finite element grid used to discretize the noise. Then, if finite element interpolation is used in space and piecewise linear interpolation is used in time, we would have that the discretized noise appearing on the right-hand side of (20) is given by, for $\hat{n} = 0, 1, 2, \ldots$,

$$\eta_{\hat{h},\hat{\Delta}t}(\mathbf{x}, t) = \sum_{\hat{\jmath}=1}^{\hat{J}} \left(\frac{(t - t_{\hat{n}+1})\mu_{\hat{\jmath},\hat{n}+1} + (t_{\hat{n}} - t)\mu_{\hat{\jmath},\hat{n}}}{\hat{\Delta}t} \right) \hat{\phi}_{\hat{\jmath}}^{\hat{h}}(\mathbf{x}) \quad \text{for } t \in [t_{\hat{n}}, t_{\hat{n}+1}],$$

where $t_{\hat{n}} = \hat{n}\hat{\Delta}t$, and $\{\hat{\phi}_{\hat{\jmath}}^{\hat{h}}(\mathbf{x})\}_{\hat{\jmath}=1}^{\hat{J}}$ is a basis for the finite element space $V^{\hat{h}}$ used to discretize the noise. We can now introduce quadrature rules to evaluate the integrals appearing in (20).

The finite element space used to discretize the noise is not the same as that used to discretize the partial differential equation; i.e., $V^h \neq V^{\hat{h}}$. In fact, we take the view that the spatial grid and time step used to discretize the noise are fixed with respect to refinements of the spatial grid and time step used to discretize the partial differential equation. In this approach to discretizing noise, one can determine the discretized noise before one begins the computation of the approximate solution of the partial differential equation.

4. SIMULATIONS INVOLVING SPACE–TIME-INDEPENDENT ADDITIVE NOISE

The numerical computations are based on a code developed for the steady-state and time-dependent Ginzburg–Landau models and several of their variants; see [2, 5, 9, 10, 11]. Piecewise quadratic finite element spaces on uniform meshes are used in space while a backward Euler scheme is used in the time discretization. In the figures, contour lines for the magnitude of the order parameter ψ are plotted. The square of the magnitude of the order parameter is proportional to the density of superconducting charge carriers; thus, $|\psi| = 0$ then corresponds to the normal, i.e., nonsuperconducting, state and, in our nondimensionalization, $|\psi| = 1$ corresponds to the superconducting state. Values in between correspond the "mixed state." Only those contour lines corresponding to $|\psi| \leq 0.5$ are shown and we refer to the isolated regions such that $|\psi| \leq 0.5$ as the *core regions* of the vortices and the diameters of these regions are referred to as the *core sizes* that are related to the coherence length of the material sample.

Development of a vortex lattice in the deterministic case. Recall that as vortices form through time, they nucleate at the sides of the sample and move toward the center. The vortex lattice then rotates into an *Abrikosov lattice* as seen in Fig. 1, which is for a homogeneous, isotropic, two-dimensional superconducting material of size $20\xi \times 20\xi$ in a perpendicular magnetic field of magnitude 0.5κ. (Recall that all variables have been appropriately nondimensionalized.) Here, ξ denotes the Ginzburg–Landau coherence length. In the steady-state configuration, which minimizes the Gibbs free energy, the vortices are circular in shape, are stationary in the sample, and form a regular, triangular pattern.

Development of a quasi-steady-state vortex lattice in the space–time-independent additive noise case. When additive noise is simulated, we randomly sampled the noise values at all time steps and at all grid points using independent random variables having a Gaussian distribution of zero mean. When a given noise with variance 2 is added to the same material sample as that considered in Fig. 1, the lattice no longer rotates into a steady-state lattice.

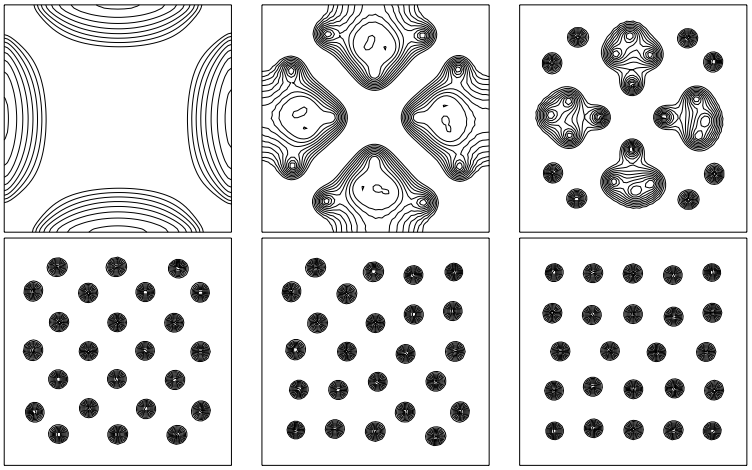

FIG. 1. Time evolution of the magnitude of the order parameter in a $20\xi \times 20\xi$ homogeneous, isotropic sample with no noise; the bottom right figure is the steady-state configuration. A rotation of the lattice occurred between the last two figures.

Instead, the vortices vibrate in the sample until a lattice similar to the lattice in Fig. 1 is formed; see Fig. 2. A lattice is recognizable in this sample, but a true steady state as seen in Fig. 1 is not achieved since the shapes of the vortices are distorted and the vortices are constantly in motion. However, with this small variance of 2, the vortices do try to form a regular, triangular pattern in the sample. We refer to the situation in which a persistent lattice is recognizable, but a true steady state is not achieved as a *quasi-steady-state* configuration. (We will discuss this notion further in Section 6.) Note that due to the presence of the additive noise, the vortices are no longer circular but that the core sizes are about the same, not only from one vortex to another, but also for the same vortex from one time instant to another.

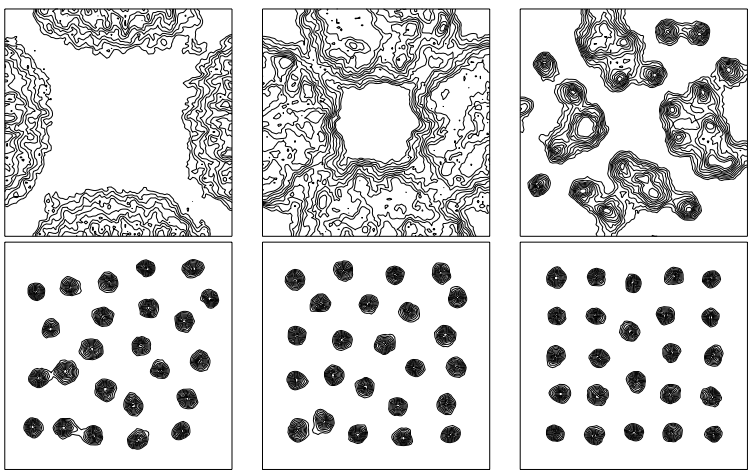

FIG. 2. Time evolution of the magnitude of the order parameter with space–time-independent additive noise of variance 2 in a $20\xi \times 20\xi$ sample. The bottom right figure corresponds to a snapshot of the quasi-steady-state configuration, i.e., one for which the motion of the vortices is essentially a vibration of their core regions.

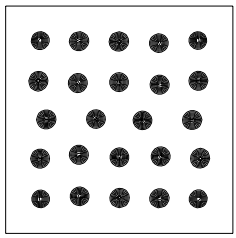

FIG. 3. Steady-state vortex lattice with no thermal fluctuations in a $20\xi \times 20\xi$ sample.

Since the forcing function η is random, different computational runs can result not only in different evolutionary histories, but also in different persistent vortex lattice patterns that appear after marching through time. For example, during the time evolution when the vortices enter the sample, the presence of noise can inhibit some vortices from entering. Three computational runs were performed with the same material, the same magnetic field, and the same variance of 2 for the additive noise. Three different quasi-steady states were observed in the separate computations; these correspond to noise terms η that are three different realizations of the same random Gaussian distribution. One can compare the steady-state lattice in Fig. 3 for the no noise case to the three realizations of the quasi-steady-state vortex lattices in Fig. 4. The middle configuration of Fig. 4 for the additive noise case has the same number of vortices as that for the no noise case of Fig. 3, but the lattice is rotated 90°. The left and right plots of Fig. 4 display lattices that only have 23 vortices compared to the 24 vortices in the steady-state lattice without noise (see Fig. 3). One vortex is inhibited from entering the material during the nucleation process at the boundary of the sample due to the presence of noise in the model. The two lattices with 23 vortices are similar to each other with a relative 90° rotation of the lattice structure.

Effect of increasing the variance. As was mentioned previously, the variance is inversely related to the difference between the temperature and the critical temperature of transition between the superconducting and normal states. The closer one is to the critical temperature, the greater are the effects of thermal fluctuations and, in the nondimensionalized models we are using, the larger is the variance of the noise term. In Fig. 5, snapshots taken at the same instant of time for different values of the variance are compared for a $20\xi \times 20\xi$ sample. The upper-left plot is for zero variance, i.e., the deterministic case. The remaining plots result from a series of calculations with variances equal to $1, 2, \ldots, 10$. At first, vortices are recognizable and a vortex lattice is seen in the material. As the temperature is increased (and correspondingly, the variance as well), the vortices are no longer recognizable and neither is a vortex lattice. In Fig. 6, we give a similar set of plots for a three-dimensional computation.

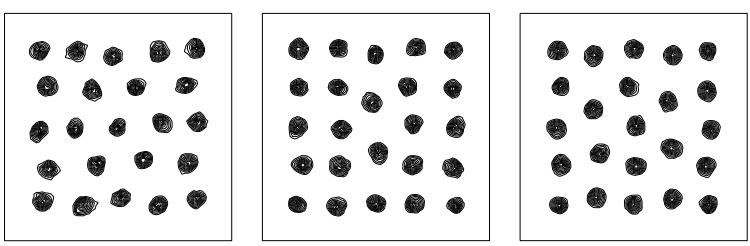

FIG. 4. Three realizations of the quasi-steady-state vortex lattice in the presence of additive noise in a $20\xi \times 20\xi$ sample. All realizations are for the same variance of 2 for the additive noise.

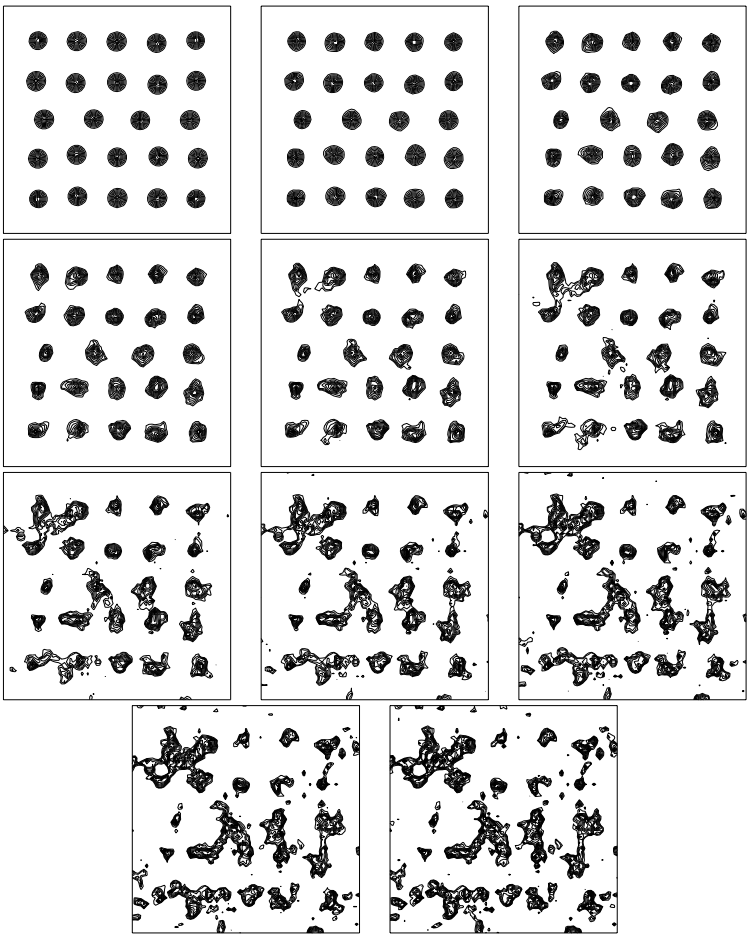

FIG. 5. Snapshots in time of the magnitude of the order parameter for a $20\xi \times 20\xi$ sample with space–time-independent additive noise having variances of 0 to 10. All snapshots are taken at the same time instant.

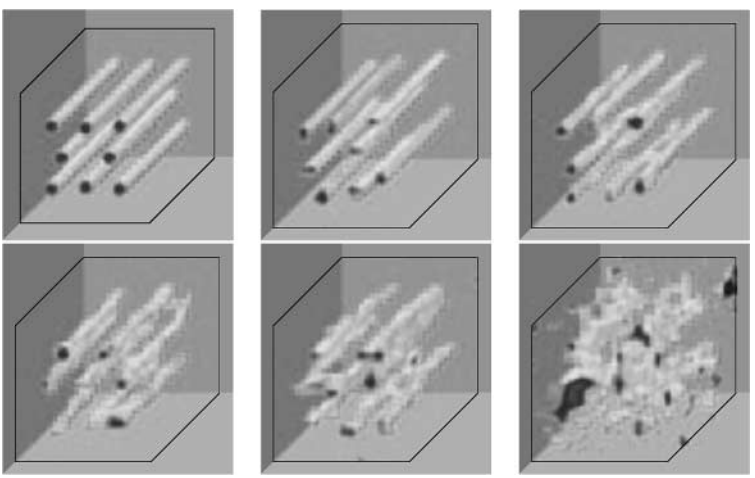

FIG. 6. Snapshots taken at the same time instant of the magnitude of the order parameter for a $15\xi \times 15\xi \times 15\xi$ sample with space–time-independent additive noise having variances $= 0, 2, 5, 7, 8,$ and 15.

The variance parameter controls the level of noise that is added to the time-dependent Ginzburg–Landau equations. As the variance increases, the vortices are more distorted and eventually vortices are not recognizable. As was seen in Fig. 4, different *quasi-steady states* can arise from calculations with the same variance level due to different realizations of the stochastic process that models, e.g., thermal fluctuations. However, although for the same value of the variance the details of the different realizations may vary (even the number of vortices may be different), the level of distortion of the vortices and the vortex lattices are very similar; e.g., the level of disorder of the individual vortices and of the lattice are similar.

The results of the numerical simulations are in qualitative agreement with the experimental results of [17]. It is, of course, well known (see, e.g., [22]) that for a fixed value of the applied field, as the temperature is increased, there is a transition from the Abrikosov state (a regular, triangular lattice of vortices) to the normal state (in which superconductivity is suppressed so that $|\psi| = 0$). In [17], convincing evidence was presented that due to thermal fluctuations, this transition is not a sharp transition. Indeed, before superconductivity is completely suppressed, the regular vortex lattice of the Abrikosov state (the *vortex-glass state*) is first disordered into the *vortex-liquid state* for which no lattice is recognizable. From Figs. 5 and 6, we see that this is exactly what happens in the numerical simulations as the value of the variance is increased, i.e., as the temperature approaches the transition temperature. For low values of the variance, a recognizable lattice of vortices persists; however, for high values of the variance, i.e., for temperatures close to the transition temperature, the vortex lattice is destroyed although superconductivity, i.e., points in the sample for which $|\psi| \neq 0$, persist.

One other important feature of the experimental results of [17] is also present in the numerical simulations. In [17], the experimental data showed that for a constant applied magnetic field, the vortex-liquid state occurred over a narrow range (relative to the transition temperature itself) of temperatures near the transition temperature. Thus, the vortex-glass state, i.e., the recognizable lattice of discrete vortices, persisted for temperatures quite near the transition temperature and that the vortex-liquid state existed for only a narrow band of temperatures near the transition temperature. This qualitative feature of the vortex-liquid state is also present in the numerical simulations. For example, from Fig. 5, we see that the vortex lattice remains recognizable up to values of the variance of about 5; this corresponds to the vortex-liquid state existing for a band of temperatures of approximately 0.2 K near the transition temperature; this is in rough agreement with the experimental results of [17].

5. COMPUTATIONS INVOLVING MULTIPLICATIVE NOISE

We next present some computational simulations for the multiplicative noise case discussed in Section 2.2.

Space–time-independent multiplicative noise. We first consider noise that is independent in space–time so that the discretized noise is essentially sampled on the same grid as that used for the discretization of the Ginzburg–Landau equations. In spatial directions, the size of this grid is much smaller than a coherence length.

The material sample has dimension $10\xi \times 10\xi$ and the applied field $H = \text{curl}\,\mathbf{A} = 0.5\kappa$. (Recall that all variables have been appropriately nondimensionalized.) Contour plots of the magnitude of the order parameter are given in Figs. 7 and 8 for values of the variances

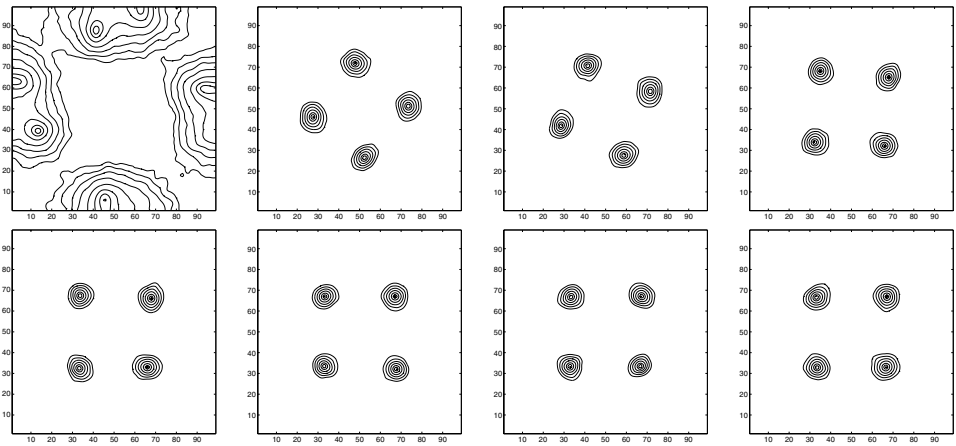

FIG. 7. Level curves of the magnitude of the order parameter for a $10\xi \times 10\xi$ sample with space–time-independent multiplicative noise having variance $= 4$ at times $=$ 5, 20, 60, 120, 180, 240, 300, and 360.

equal to 4 and 8, respectively. Again, only contour curves corresponding to $|\psi| \leq 0.5$ are shown. For comparison purposes, in Fig. 9, we present the contour plots of the magnitude of the order parameter for the deterministic high-κ model. There are noticeable decreases in core sizes for larger values of the variance while the relative motion of the centers of the vortices are less dramatic than for the additive noise case.

Correlated multiplicative noise. We next consider some computations for multiplicative noise in which the noise is sampled on a space–time grid of the scale of a coherence length, i.e., one much coarser than that used to discretize the Ginzburg–Landau equations. Some interesting phenomena develop as the less frequent sampling decreases the variations of the coefficients in the source term and thus gives rise to the change of the effective coherence length over time and space. One can observe that the cores of the vortices undergo constant expansion and shrinkage. For example, consider Figs. 10 and 11 in which a $15\xi \times 15\xi$ sample with multiplicative noise sampled over a lattice of dimension of a coherence length is considered. In Fig. 10, we follow the nucleation of vortices at the boundary of the sample

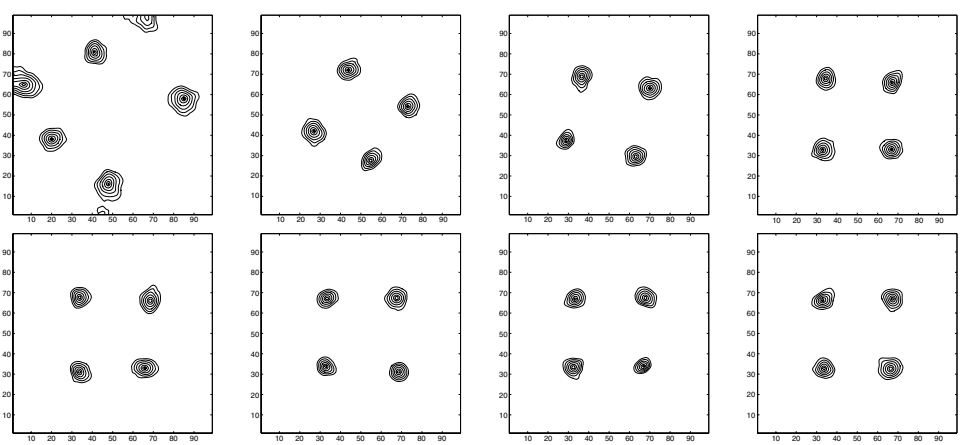

FIG. 8. Level curves of the magnitude of the order parameter for a $10\xi \times 10\xi$ sample with space–time-independent multiplicative noise having variance $= 8$ at times $=$ 5, 20, 60, 120, 180, 240, 300, and 360.

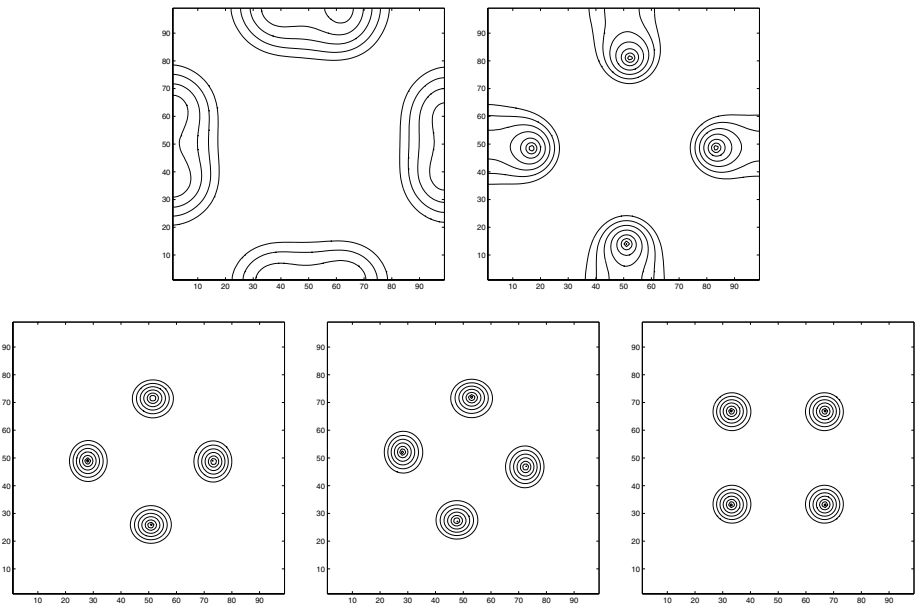

FIG. 9. Level curves of the magnitude of the order parameter for a $10\xi \times 10\xi$ sample with no noise at time $=$ 1, 5, 10, 15, 25, 95 and the steady state.

and the subsequent migration of the vortices to their quasi-steady-state positions. In Fig. 11, we follow the vortices after the quasi-steady state has been established. We see that not only are the vortex centers moving significantly, but also that the sizes of the vortex cores change dramatically in time. Furthermore, at the same time, different vortices can have widely different core sizes.

We note that these calculations with multiplicative noise with long-range order may be most relevant to modeling the effect of random inhomgenieties in the material sample; in this case, randomness occurs over scales that may be comparable to the coherence length and therefore may be modeled by sampling over lattices that are large with respect to the

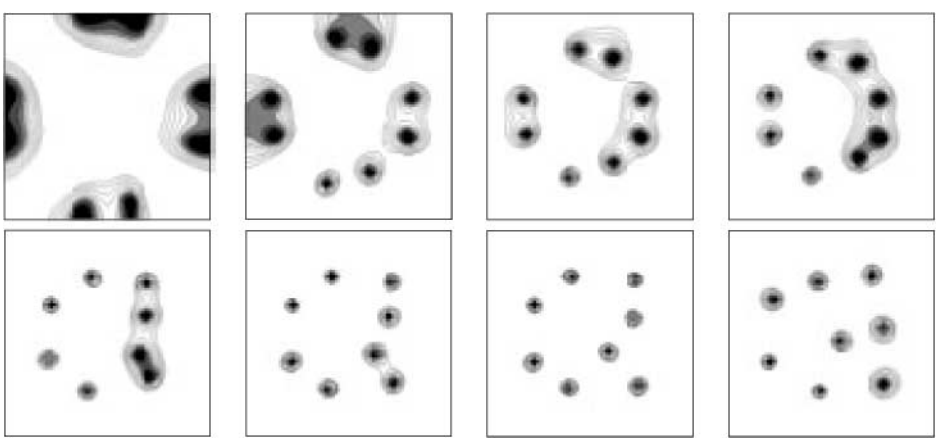

FIG. 10. Level curves of the magnitude of the order parameter for a $15\xi \times 15\xi$ sample with multiplicative noise having long-range order during the vortex nucleation process.

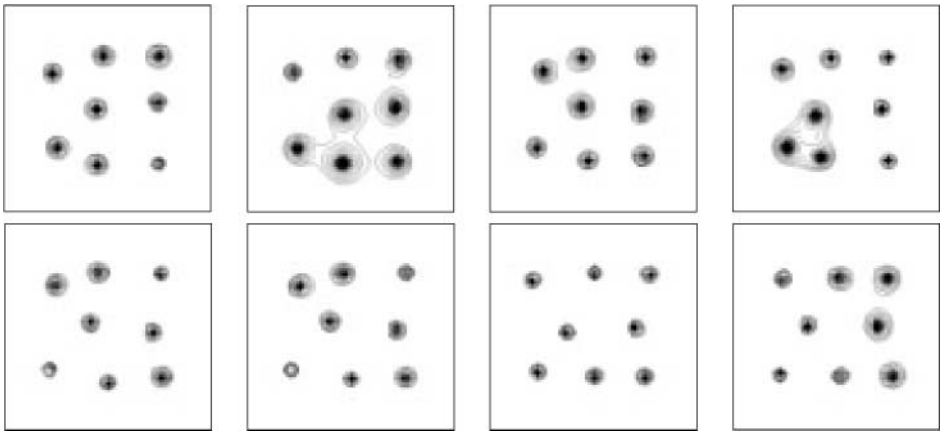

FIG. 11. Level curves of the magnitude of the order parameter for a $15\xi \times 15\xi$ sample with multiplicative noise having long-range order after a quasi-steady-state lattice has been established.

grid lengths used in the computations. Of course, inhomogenieties in the material sample cause the pinning of the vortex lattice so that by modeling random inhomegenieties, one is also modeling pinning effects in inhomogeneous superconductors.

6. LARGE TIME BEHAVIOR

A question remains to be answered: can the vortex lattice that appears in the time evolution of superconductors under the presence of noise be considered to be a type of *steady-state* lattice, at least on average?

In Figs. 12 and 13, we present the free energy vs time for simulations of both the additive and multiplicative noise cases, respectively, for a $10\xi \times 10\xi$ sample; variances of 4, 8, and 16 are considered for the noise. (Throughout this section, both multiplicative and additive

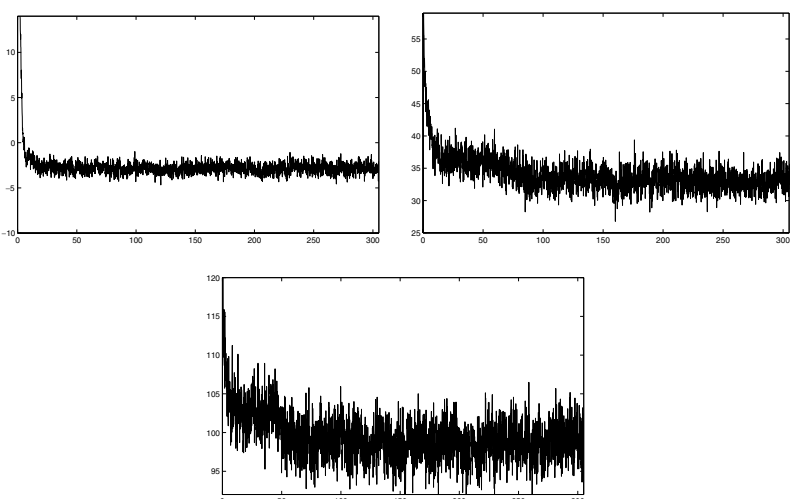

FIG. 12. The Gibbs free energy vs time for the additive noise case in a $10\xi \times 10\xi$ sample with variances $= 4$, 8, and 16.

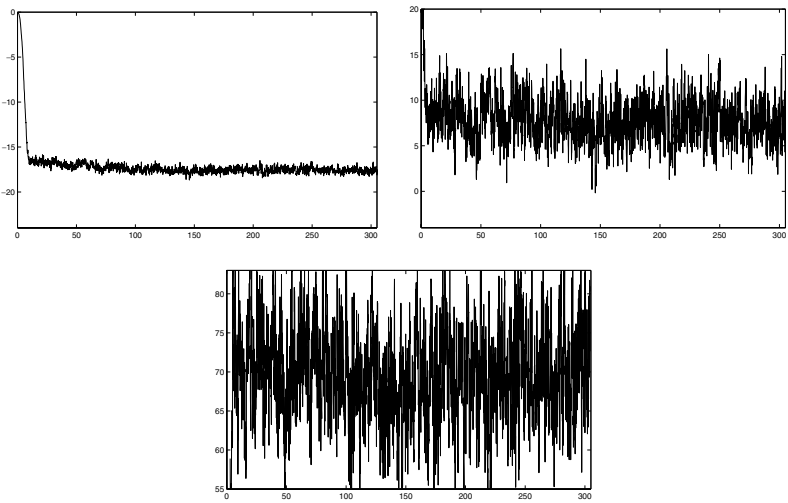

FIG. 13. The Gibbs free energy vs time for the multiplicative noise case in a $10\xi \times 10\xi$ sample with variances = 4, 8, and 16.

noise functions are considered to be independent in space and time so that the discretized noise is sampled essentially on the same space–time grid as that used to discretize the differential equations.) In Fig. 14, we give the free energy vs time for the no noise case. Comparing Figs. 12 and 13 with Fig. 14, we see that in the presence of noise, the random motion of the vortices results in oscillations in the value of the free energy. (The ordinates of all the plots in Figs. 12–14 have the same scaling factors of 25 units.) The much larger oscillations associated with the multiplicative noise cases are perhaps due to the dramatic change of core sizes and for the case of variance being equal to 16, the largest magnitude of the order parameter can be as high as 1.6, compared with 1 being the upper bound in the deterministic case.

We may, however, define the *quasi-steady state* as a state in which the vortices are *on average* in a steady-state lattice. Given a pathwise solution $f = f(t)$, the averages $\bar{f}_T = \bar{f}(t)$ are taken over time intervals of the form $[t + jT, t + (j + 1)T]$ for some T of reasonable length. On the other hand, we define $\hat{f}(t)$ to be the steady-state solution of the corresponding noiseless dynamic equations with $f(t)$ as the initial condition (or

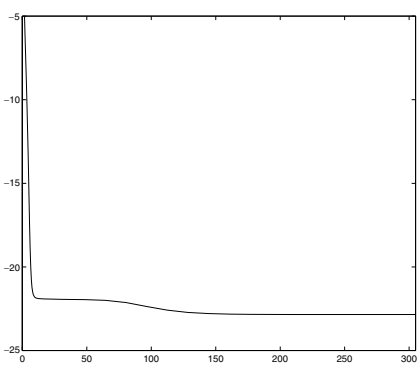

FIG. 14. The Gibbs free energy vs time for the no noise case (variance = 0) in a $10\xi \times 10\xi$ sample.

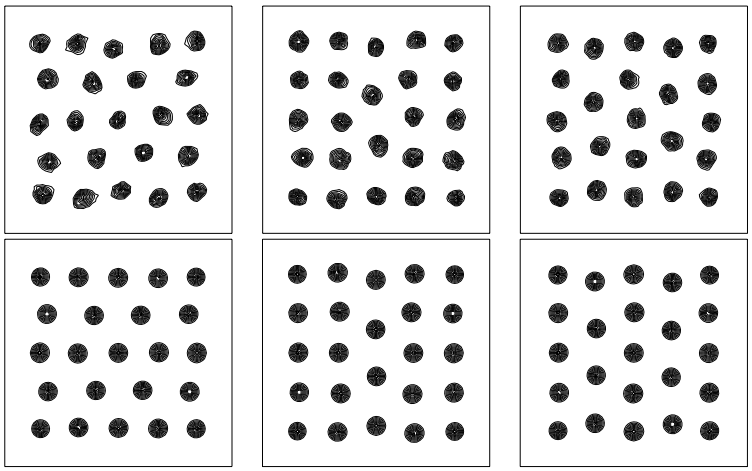

FIG. 15. Comparison of quasi-steady-state lattices to steady-state lattices in a $20\xi \times 20\xi$ sample for additive noise having variance 2. Each of the snapshots of the computation with noise in the upper row were used as an initial condition for a deterministic computation. In each case, the latter achieved a steady state which is depicted in the bottom row.

equivalently, we continue solving the equations for f after time t with the noise being "turned off" and let time go to infinity). If as j goes to infinity, the averaged solution $\bar{f}_T(t)$ approaches the noiseless steady state $\hat{f}(t)$, then we say the solution f is in a *quasi-steady state*. In materials or at temperatures resulting in small variance fluctuations, a *quasi-steady state* can be seen since the vortices are allowed to be in constant motion with their average position defining the *quasi-steady-state* lattice.

One can show that the three vortex lattices in Fig. 4 are quasi-steady states. In fact, by shutting off the noises at large time, the steady states match with some local minimizers of the Gibbs free energy with the given number of vortices present in the superconductor. One can compare the steady-state lattice obtained from these calculations to the vortex lattices that appear under the presence of noise. In Fig. 15, one can see that the vortices in the models with noise are on average in the correct lattice formation. The top row of plots corresponds to the same nondimensional time in three different computations with the variance set to 2. The bottom row of plots corresponds to the resulting steady-state lattices observed after noise is "turned off" in the three previous computations. Thus, the three vortex lattices obtained from different realizations of the time evolution with noise having a variance of 2 can be classified as leading to a quasi-steady state.

Note that in [14], the average position of vortices is determined by averaging the equations that determine the movement of vortices, i.e., equations involving ψ and $\mathbf{A}$. The resulting equations are necessarily stochastic in nature meaning that the position of vortices in a sample at a particular time t is not completely determined by the initial condition of the sample at $t = 0$.

7. THE LARGE TIME BEHAVIOR AND THE SMALL VARIANCE LIMIT

We now consider some theoretical issues related to the stochastic models we have been using. We refer to [1, 3, 4, 12, 19] for more comprehensive mathematical treatments of stochastic partial differential equations.

Let $\mathcal{H} = L^2(\Omega)$ be the space of all square integrable complex-valued functions defined on Ω. Assuming that $\mathbf{A}$ is smoothly defined and uniformly bounded, it is easy to check that the differential operator $\hat{A}_0$ defined by (10) on the domain

$$D(\hat{A}_0) = \{u \in H^2(\Omega)(\text{the complex version}) \text{ and } u \text{ satisfying (11)}\}$$

can be extended to $\hat{A}_0 : V \to V^*$ with $V = D(\hat{A}_0^{I/2})$, where V^* denotes the dual space. Let $\langle .,. \rangle$ be the duality pairing between V and V^* which is equivalent to the scalar product in $\mathcal{H}$. It is easy to see that $\hat{A}_0$ is an operator with

$$\|\hat{A}_0\|_{L(V,V^*)} \leq a_1$$

for some constant a_1 and

$$\langle u, \hat{A}_0 u \rangle \geq 0$$

for any $u \in V$. We use the standard notation $\|\cdot\|$ for the standard L^2 norm in $\mathcal{H}$.

Given a complete probability space $(\Lambda, \mathcal{F}, P)$, and an increasing filtration of σ-fields $\mathcal{F}_t \subset \mathcal{F}$ containing all P-null sets of Λ, let $M_T^2(V)$ denote the space of all V-valued measurable processes u satisfying

$$u(t, .) \text{ is } \mathcal{F}_t - \text{measurable} \quad \text{and} \quad E\int_0^T \|u(t,\omega)\|_V^2 \, dt \text{ is finite.}$$

Let $W(t), t \geq 0$ be a $\mathcal{H}$-valued Wiener process with covariance operator $\mathcal{Q}$, which is a Hilbert–Schmidt operator. For the sake of theoretical investigations, we also assume that the trace of $\mathcal{Q}$ is finite. Naturally, these assumptions limit the types of noises to which the theoretical results given here are applicable.

We can consider stochastic differential equations of the form

$$du(t) = A(u(t))\, dt + B(u(t))\, dW(t) \tag{21}$$

and the solution refers to the process $u \in M_T^2(V)$ that satisfies the above equation and a suitable initial condition.

Based on the theory given in [18], with Hilbert spaces $V \subset \mathcal{H} \subset V^*$ and V compactly embedded in $\mathcal{H}$, it follows that there exists a unique solution $\{u^\varphi, t \geq 0\}$ of the equation (21) such that

$$u^\varphi \in L^2(\Lambda, C(0, T; \mathcal{H})) \cap M_T^2(V)$$

under the following assumptions: there exist $\alpha > 0$, λ, and γ such that $\forall v \in V$

$$2\langle v, A(v)\rangle + \text{tr}(B(v)\mathcal{Q}B^*(v)) \leq \lambda\|v\|_{\mathcal{H}}^2 - \alpha\|v\|_V^2 + \gamma$$

and $\forall u, v \in V$

$$2\langle (u - v, A(u) - A(v))\rangle + \text{tr}((B(u) - B(v))\mathcal{Q}(B(u) - B(v))^*) \leq \lambda\|u - v\|_{\mathcal{H}}^2,$$

where $\langle\, , \rangle$ denotes the duality pairing for V and V^*.

The solution of the additive stochastic high-κ model refers to the process $u_\sigma \in M_T^2(V)$ that satisfies Eq. (21) with $A = \hat{A}_0 + F$ and $B(u) = \sigma$ for $u \in V$ while the multiplicative case corresponds to $A = \hat{A}_0 + F$ and $B(u) = \sigma u$. Using the monotonicity of the nonlinear function F and the coercivity of $\hat{A}_0$, one can easily verify that the conditions for the existence and uniqueness of solutions are satisfied. Moreover, it is easy to see that Eqs. (7) and (12) can be respectively classified as dissipative equations with additive noise and linear multiplicative noise [4] and consequently the existence and uniqueness of generalized solutions to the stochastic equations can be established.

It also follows from [4] that, for the additive noise case, there exists one unique invariant measure for (7). One may also study the small variance limits; that is, let $u_0(t) \in V$ be the solution to the *deterministic* differential equation

$$du_0(t) = \hat{A}(u_0(t))\,dt \tag{22}$$

with initial condition (8)—i.e., $u(t) = \psi(t)$, the solution given by (1). Then, for the error $e(t) = u_\sigma(t) - u_0(t)$, we have

$$de(t) = [\hat{A}(e(t) + u_0(t)) - \hat{A}(u_0(t))]\,dt + B(e(t) + u_0(t))\,dW(t). \tag{23}$$

Applying the techniques given in [4], one can show that as the parameter σ goes to zero,

$$E\|e(t)\|^2 \to 0 \quad \text{as } \omega \to 0.$$

We give a brief proof for such a result based on the well-known Ito formula [4, 18]. Let $\Psi : \mathcal{H} \to R$ be a function satisfying:

1. Ψ is twice (Frechet) differentiable with Ψ' and Ψ'' locally bounded;
2. Ψ, Ψ' are continuous on $\mathcal{H}$;
3. for all trace class operators P, $\mathrm{tr}(P\Psi'(\cdot))$ is continuous for each $v^* \in V^*$;
4. $\|\Psi'(v)\|_V \le C_0(1 + \|v\|_V)$ for some $C_0 > 0, \forall v \in V$.

Then,

THEOREM 7.1 (Ito's formula). *Suppose $\Psi : \mathcal{H} \to R$ satisfies the above conditions and $\{u^\varphi(t), t \ge 0\}$ is a solution of (21) with $u^\varphi \in L^2(\Omega, C(0, T; H)) \cap M^2(0; T; V)$.*

Then,

$$\Psi(u^\varphi(t)) = \Psi(u^\varphi(0)) + \int_0^t L\Psi(u^\varphi(s))\,ds + \int_0^t (\Psi'(u^\varphi(s)), B(u^\varphi(s))\,dW(s)),$$

where $L\Psi(u) = \langle \Psi'(u), A(u)\rangle + \frac{1}{2}\mathrm{tr}(\Psi''(u)B(u)QB^*(u))$, and Q is the covariance.

We now take $\Psi(e) = \|e\|^2$, and for the additive noise case, it is straightforward to check that

$$L\Psi(u^\varphi(s)) = 2Re\left\{ \int_\Omega \langle e(s), a(e, s)\rangle\,d\Omega \right\} + \int_\Omega \omega^2 \,\mathrm{tr}\,\mathcal{Q}\,d\Omega,$$

where $a(e, s) = \hat{A}_0(e(t)) + F(u_0(t) + e(t)) - F(u_0(t))$. Meanwhile, it is also easy to obtain that

$$Re\{(F(u_\sigma) - F(u_0), u_\sigma - u_0)\} \ge 0 \tag{24}$$

and

$$Re\{\langle e, \hat{A}_0(e)\rangle\} \le \|e\|^2. \tag{25}$$

Thus, we have

$$E(\|e(t)\|^2) = E\left(\|e(0)\|^2 + \int_0^t \|e(s)\|^2\, ds + \sigma \int_0^t e(s)\, dW(s)\right). \tag{26}$$

As the initial conditions for u_σ and u are the same, we get $e(0) = 0$. By the Birkholder–Gundy inequality [1], we have

$$\sigma E\left(\int_0^t e(s)\, dW(s)\right) \le c\sigma^2 \operatorname{tr}(\mathcal{Q}) + E\left(\int_0^t \|e(s)\|^2\, ds\right)$$

for some positive constant c. So,

$$E(\|e(t)\|^2) \le E\left(\int_0^t \|e(s)\|^2\, ds\right) + c\sigma^2 \operatorname{tr}(\mathcal{Q}). \tag{27}$$

Using Fubini's theorem to switch integration order, we arrive at

$$E(\|e(t)\|^2) \le \int_0^t E(\|e(s)\|^2)\, ds + c\sigma^2 \operatorname{tr}(\mathcal{Q}). \tag{28}$$

Then, by the Gronwall's inequality, we have the following results.

THEOREM 7.2. *Let $u_0(t)$ be the solution to the deterministic differential equation* (22) *and let $u_\sigma(t)$ be the solution to the stochastic differential equation* (7). *Then, for any $T > 0$,*

$$\sup_{t\in[0,T]} E\|u_\sigma(t) - u_0(t)\|^2 \le C\sigma^2 \operatorname{tr}(\mathcal{Q}) \quad \textit{for some constant } C$$

and, consequently,

$$\sup_{t\in[0,T]} E\|u_\sigma(t) - u_0(t)\|^2 \to 0 \quad \textit{as } \sigma \to 0.$$

The case for the multiplicative noise is more involved and we omit the details. The above theorem establishes the relations between the time evolution of the deterministic model and the model with the noise effects. It confirms, to a certain degree, the observations we made from the numerical simulations for the additive noise case presented earlier; i.e., as the variance parameter σ gets smaller, the *quasi-steady-state lattice* that develops in the presence of noise converges to the *steady-state lattice* obtained in calculations without noise. We observe that, rigorously speaking, the noise we have taken in the numerical experiments does not strictly simulate the Wiener process $W(t)$ whose covariance operator is of trace class in $\mathcal{H}$.

8. SUMMARY AND CONCLUSIONS

Computationally, the effects of thermal fluctuations or random defects are evident in contour plots of the density of superconducting electrons since vortices are in constant motion, the vortices are distorted, and the resulting vortex lattice is also distorted. With small variances and at large times, the vortices seem to be at an equilibrium where each vortex is on the *average* at a fixed position in the sample. When noise is subsequently suppressed at this *quasi-steady state*, the resulting vortex lattice evolves into a steady-state configuration for the sample with respect to the number of vortices present in the material. Although a sample can have several different steady-state lattice structures corresponding to different realizations of the same stochastic process with a given variance, each lattice is a quasi-steady state. Thus, the lattice symmetry and regularity seen in pure materials without thermal fluctuations or random defects are still seen with the addition of noise in our model. We also observe that while additive noise tends to make the positions of vortices vibrate, multiplicative noise (having long-range order) tends to alter the core sizes of the vortices, which is even more apparent when discrete lattice random functions are used.

Theoretically, it is also shown that as the variance approaches zero, the solution of the stochastic high-κ time-dependent Ginzburg–Landau equations approaches the solution of the deterministic high-κ time-dependent Ginzburg–Landau equations. When the variance decreases to zero, the level of noise introduced to the stochastic time-dependent Ginzburg–Landau equation goes to zero. Intuitively, as the level of noise goes to zero, the resulting values of ψ at the steady state should approach the values obtained without fluctuations. Therefore, this theoretical result is reflected in the computational studies of quasi-steady-state lattices.

While in the present paper most of the numerical examples involve relatively few vortices, it is also of great physical interest to pursue further study in the future on the effect of thermal fluctuation when a large number of vortices are present. Another avenue for future work is to include the effects of applied currents; this would allow for the study of the pinning of the vortex lattice due to random inhomogenieties in the material sample and of the critical current at which depinning takes place.

REFERENCES

1. R. Carmona and B. Rozovskii (Eds.), *Stochastic Partial Differential Equations: Six Perspectives* (Am. Math. Soc., Providence, 1998).
2. J. Chapman, Q. Du, M. Gunzburger, and J. Peterson, Simplified Ginzburg–Landau models for superconductivity valid for high Kappa and high fields, *Adv. Appl. Math.* **5**, 193 (1995).
3. L. Chow, J. Jiang, and J. Menaldi, Pathwise convergence of approximate solutions to Zakai's equation in a bounded domain, in *Stochastic Partial Differential Equations and Applications*, edited. by G. Prato and L. Tibaro (Wiley, New York, 1992), p. 111.
4. G. Da Prato and J. Zabczyk, *Stochastic Equations in Infinite Dimensions* (Cambridge Univ. Press. Cambridge, 1992).
5. J. Deang, Q. Du, M. Gunzburger, and J. Peterson, Vortices in superconductors: Modeling and computer simulations, *Philos. Trans. Roy. Soc. London Ser. A* **355**, 1957 (1997).
6. A. Dorsey, M. Huang, and M. Fisher, Dynamics of the normal to superconducting vortex-glass transition: Mean-field theory and fluctuations, *Phys. Rev. B* **45**, 523 (1992).
7. Q. Du, Finite element methods for the time dependent Ginzburg–Landau model for superconductivity, *Comput. Math. Appl.* **27**, 119 (1994).

8. Q. Du and P. Gray, High-kappa limit of the time dependent Ginzburg–Landau model for superconductivity, *SIAM J. Appl. Math.* **56**, 1060 (1996).
9. Q. Du, M. Gunzburger, and J. Peterson, Analysis and approximation of the Ginzburg–Landau model of superconductivity, *SIAM Rev.* **34**, 54 (1992).
10. Q. Du, M. Gunzburger, and J. Peterson, Solving the Ginzburg–Landau equations by finite element methods, *Phys. Rev. B* **46**, 9027 (1992).
11. Q. Du, M. Gunzburger, and J. Peterson, Computational simulations of type-II superconductivity including pinning mechanisms, *Phy. Rev. B* **51**, 16,194 (1995).
12. F. Fandoli, *Regularity Theory and Stochastic Flows for Parabolic PDEs* (Gordon & Breach, Sydney, Australia, 1995).
13. A. Filippov, A. Radievsky, and A. Zelster, Nucleation at the fluctuation induced first order phase transition to superconductivity, *Phy. Lett. A* **192**, 131 (1994).
14. P. Hohenberg and B. Halperin, Theory of dynamic critical phenomena, *Rev. Mod. Phy.* **49**, 453 (1977).
15. T. Kamppeter, F. Mertens, E. Moro, A. Sánchez, and A. Bishop, Stochastic vortex dynamics in two-dimensional easy-plane ferromagnets: Multiplicative versus additive noise, *Phys. Rev. B* **43**, 5992 (1991).
16. A. Larkin, Effect of inhomogeneities on the structure of the mixed state of superconductors, *Sov. Phys. JETP* **31**, 784 (1970). [English translation]
17. X. Ling, S. Park, B. McClain, S. Choi, D. Dender, and J. Lynn, Superheating and supercooling of vortex matter in a Nb single cystal: Direct evidence for a phase transition at the peak effect from neutron diffraction, *Phys. Rev. Lett.* **86**, 712 (2001).
18. E. Pardoux, Stochastic partial differential equations and filtering of diffusion processes, *Stochastics* **3**, 127 (1979).
19. B. Rozovskii, *Stochastic Evolution Systems: Linear Theory and Applications to Non-linear Filtering* (Kluwer, Dordrecht, 1990).
20. R. Sasik, L. Bettencourt, and S. Habib. Thermal vortex motion in a two-dimensional condensate, *Phys. Rev. B* **62**, 1238 (2000).
21. W. Skocpol and M. Tinkham, Fluctuations near superconducting phase transitions, *Rep. Progr. Phys.* **38**, 1049 (1975).
22. M. Tinkham, *Introduction to Superconductivity* (McGraw-Hill, New York, 1975).
23. R. Troy and A. Dorsey, Transport properties and fluctuations in type-II superconductors near Hc2, *Phys. Rev. B* **47**, 2715 (1993).
24. S. Ullah and A. Dorsey, The effect of fluctuations on the transport properties of type-II superconductors in a magnetic field, *Phys. Rev. B* **44**, 262 (1991).